Estimation of Background Medium's Properties in Microwave Holographic Imaging

Hailun Wu
Department of Electrical and Computer Engineering
New York Institute of Technology
New York, USA
hwu28@nyit.edu

Reza K. Amineh
Department of Electrical and Computer Engineering
New York Institute of Technology
New York, USA
rkhalaja@nyit.edu

2021 IEEE 21st Annual Wireless and Microwave Technology Conference (WAMICON) | 978-1-7281-5176-2/20/$31.00 ©2021 IEEE | DOI: 10.1109/WAMICON47156.2021.9443615

***Abstract*— In this paper, an approach is proposed to enhance the images produced by holographic microwave imaging technique. The approach estimates the electrical properties of the background medium. For that, first, we assumed that the background properties are within a pre-known range. Then, wideband holographic imaging technique is applied to two sets of frequencies to reconstruct two sets of images for assumed property values within the pre-determined range. An error is computed to record the differences between the two sets of images. The error is expected to be minimum at the true values of the background medium's properties. Simulation and experimental results demonstrate the validity of the proposed technique.**

Keywords— Image reconstruction, microwave holography, near-field microwave imaging.

I. INTRODUCTION

Recently, microwave imaging techniques have been proposed for various applications including biomedical imaging (e.g., see [1]), concealed weapon detection (e.g., see [2]), wall or through-the-wall imaging (e.g., see [3]), nondestructive testing (NDT) (e.g., see [4]), etc. One of the prominent and mature applications is holographic millimeter wave security screening of the passengers in the airports [5] providing robust and fast three-dimensional (3D) images. Recently, holographic imaging has been extended to near-field applications [6].

In microwave imaging, typically, the background medium is assumed to be homogenous with pre-known values of electrical properties. However, in practice, there are uncertainties in knowing the exact electrical properties of the background medium, which leads to degradation of the image quality in microwave imaging of hidden objects. This necessitates the development of new algorithms to estimate the effective values of ε and σ for better image reconstruction.

Here, we present a technique to estimate the electrical properties of the background medium in microwave holographic imaging. The simulation and experimental results demonstrate the validity of the proposed technique.

II. THEORY

Fig. 1 illustrates a typical microwave holographic imaging setup in which back-scattered data is acquired over a rectangular aperture. This setup includes a transmitter antenna that illuminates the object with wideband microwave power while moving over the aperture. At each position (x, y), the scattered field is recorded by the same antenna or a receiver antenna that moves together with the transmitter antenna. The back-scattered fields due to the objects are obtained and denoted by $E^{sc}(x, y, f)$ by subtracting the responses recorded without the presence of the objects from the responses recorded with the presence of the objects. These are referred to as *calibrated responses*. By the acquisition of the data at N_f frequencies, the contrast functions for the objects under test (OUT) $c_i(x, y)$ are reconstructed over $z = z_i$ planes, where $i = 1,\ldots, N_z$.

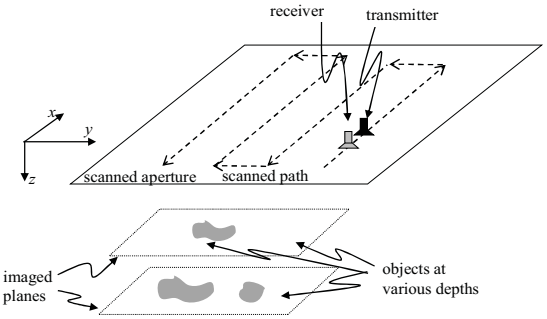

Fig. 1. Illustration of a wideband 3D microwave holographic imaging setup.

In near-field holographic imaging [6], using the convolution theory, first the point-spread function (PSF) of the system is measured or simulated *a priori*, with the assumption that the type and properties of the background medium are completely known. In practice, the acquisition of PSFs can be achieved by recording the responses for point-wise objects called calibration objects (COs). These are the smallest objects with the largest contrast that can be measured by the system and approximately represent an impulse function (Dirac delta function) as an input to the imaging system. We denote the PSF measured or simulated *a priori* using COs one at a time over each $z = z_i$ plane at frequency f as $E_i^{sc,co}(x, y, f)$.

As shown in [6], the total response $E^{sc}(x,y,f)$ measured by the receiver antenna due to the OUTs is written as the superposition of responses produced by objects on all planes:

$$E^{sc}(x,y,f)=\sum_{i=1}^{N_z}E_i^{sc}(x,y,f)=\sum_{i=1}^{N_z}E_i^{sc,co}(x,y,f)*_x*_y c_i(x,y) \quad (1)$$

where $*_x$ and $*_y$ denote convolution along x and y directions, respectively. In (1), $E^{sc}(x,y,f)$ function is known by measuring of the OUT's response. In order to estimate the contrast functions $c_i(x,y)$ of OUTs, the scattered waves are recorded at multiple frequencies, f_l, l = 1,…, N_f. Then, re-writing (1) at all frequencies leads to the following system of equations:

$$\begin{cases} E^{sc}(x,y,f_1)=\sum_{i=1}^{N_z}E_i^{sc,co}(x,y,f_1)*_x*_y c_i(x,y) \\ \vdots \\ E^{sc}(x,y,f_{N_f})=\sum_{i=1}^{N_z}E_i^{sc,co}(x,y,f_{N_f})*_x*_y c_i(x,y) \end{cases} \quad (2)$$

To solve for unknowns $c_i(x,y)$, we can take two-dimensional (2D) Fourier transform (FT) with respect to x and y variables, with k_x and k_y denoting the Fourier variables, for all the equations in (2) to obtain:

$$\begin{cases} \tilde{\tilde{E}}^{sc}(k_x,k_y,f_1)=\sum_{i=1}^{N_z}\tilde{\tilde{E}}_i^{sc,co}(k_x,k_y,f_1)\tilde{\tilde{c}}_i(k_x,k_y) \\ \vdots \\ \tilde{\tilde{E}}^{sc}(k_x,k_y,f_{N_f})=\sum_{i=1}^{N_z}\tilde{\tilde{E}}_i^{sc,co}(k_x,k_y,f_{N_f})\tilde{\tilde{c}}_i(k_x,k_y) \end{cases} \quad (3)$$

where $\tilde{\tilde{E}}^{sc}(k_x,k_y,f_l)$, $\tilde{\tilde{E}}_i^{sc,co}(k_x,k_y,f_l)$ and $\tilde{\tilde{c}}_i(k_x,k_y)$ are the 2D FTs of the functions $E^{sc}(x,y,f_l)$, $E_i^{sc,co}(x,y,f_l)$ (l = 1,…,N_f), and $c_i(x,y)$, respectively. At each spatial frequency pair (k_x, k_y), the system of equations in (3) is solved. Once this process is implemented for all variations of (k_x, k_y), $\tilde{\tilde{c}}_i(k_x,k_y)$ will be obtained. Then, a 2D image at each $z = z_i$ plane is reconstructed by taking inverse 2D FT of $\tilde{\tilde{c}}_i(k_x,k_y)$. Finally, the normalized 2D images of the OUTs at all N_z planes $|c_i(x,y)|/M$ are obtained, where M is the maximum of $|c_i(x,y)|$ for all planes and $|c_i(x,y)|$ is the magnitude of $c_i(x,y)$. By putting together all 2D slice images, a 3D image of OUTs can be obtained.

In the holographic imaging technique discussed above, the type (properties) of the background medium is assumed to be known so that the relevant PSFs can be employed in the image reconstruction process. However, in practice, uncertainty in knowing the true background medium and its properties leads to image reconstruction errors. To estimate the effective electrical properties of the background medium and enhance the image quality of the reconstructed images, an algorithm with the following steps is proposed:

1) Divide the responses acquired at all frequencies f_l, l = 1,…, N_f into two sets, f_o and f_e where $o = 1,3,\ldots,N_o$, ($N_o \le N_f$) and $e = 2,4,\ldots,N_e$, ($N_e \le N_f$).

2) Select a range of possible values for ε and σ as $\varepsilon = \varepsilon_m$, m = 1,…,N_ε and $\sigma = \sigma_n$, n = 1,…, N_σ.

3) Use the two sets of responses at frequencies f_o and f_e and apply holographic imaging algorithm on them separately, employing the PSFs collected for assumed (ε_m, σ_n) pair, to obtain two sets of images, $I_1^{(m,n)}(x,y,z_i)$ and $I_2^{(m,n)}(x,y,z_i)$.

4) Evaluate the difference between the 3D images $I_1^{(m,n)}$ and $I_2^{(m,n)}$ for (ε_m, σ_n) pair in step 3 by computing the total error E_T as the sum of 2-norm of the difference between the images at all depths z_i as:

$$E_T(m,n)=\sum_{i=1}^{N_z}\| I_1^{(m,n)}(x,y,z_i)-I_2^{(m,n)}(x,y,z_i)\| \quad (4)$$

where $\|\cdot\|$ is the 2-norm operator.

5) Determine the true values of (ε, σ) as (ε_m, σ_n) where $E_T(m,n)$ is the lowest. This indicates that the images obtained from the two sets of responses are the most consistent when they are reconstructed with the true values of electrical properties.

III. Results

Here, we validate the proposed property estimation technique via simulation and experimnetal results.

A. Simulation Results

The simulation studies are performed via FEKO software in the frequency range of 3 GHz to 10 GHz with steps of 0.5 GHz. The OUTs are five spheres with radii of $r = 2$ mm and properties of $\varepsilon_r = 20$ and $\sigma = 1$ S/m. They are placed in a background medium with properties of $\varepsilon_r = 6$ and $\sigma = 0.5$ S/m at the positions of $(0,0,-50)$, $(\pm10,0,-60)$, and $(0,\pm10,-60)$ as shown in Fig. 2. A resonant dipole antenna is scanning at h = 10 mm over a rectangular aperture with size of 10λ and with steps of 0.25λ, where λ is the wavelength at the center frequency of 6.5 GHz. The images are reconstructed over planes of $z_1 = -30$ mm, $z_2 = -40$ mm, $z_3 = -50$ mm, and $z_4 = -60$ mm. The collected responses are divided into two sets. One of them consists of frequency range of 3 GHz to 10 GHz with steps of 1 GHz while the other one includes frequency range of 3.5 GHz to 9.5 GHz with steps of 1 GHz. In a test scenario, conductivity σ of the background medium is assumed to be known and the relative permittivity ε_r is assumed to be only partially known, i.e., knowing that it is within the range of 3 to 9.

To have a realistic study, we add artificial White Gaussian noise with signal to noise ratio (SNR) of 30 dB to all the simulated responses.

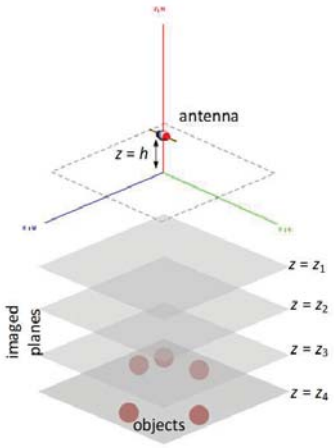

Fig. 2. Simulation setup in FEKO.

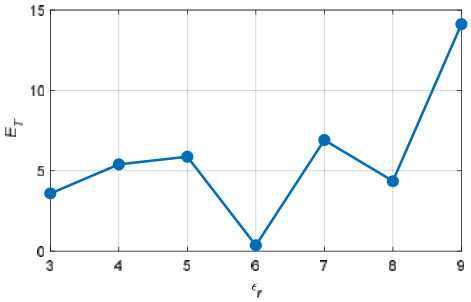

Fig. 3. Total error versus assumed permittivity values.

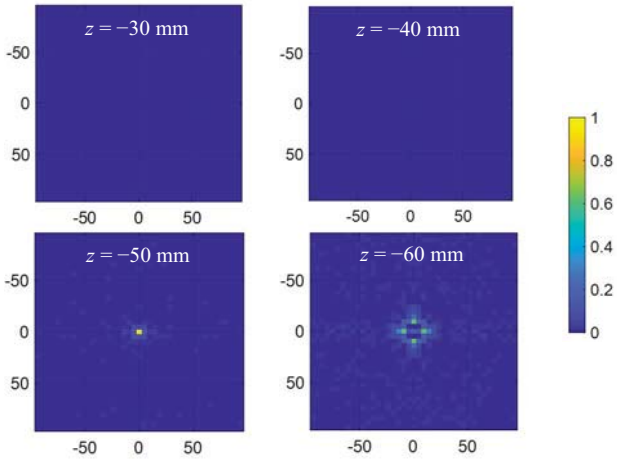

Fig. 4. Reconstructed images with the true relative permittivity value of 6. Horizontal axis: x (mm), vertical axis: y (mm).

By applying the proposed algorithm described in section II, E_T values are obtained using PSFs corresponding to various values of ε_r. Fig. 3 shows the variation of E_T values versus assumed permittivity values. It is observed that the minimum appears at $\varepsilon_r = 6$, the true value of the background medium's permittivity, as expected. Thus, images are reconstructed using the PSFs corresponding to $\varepsilon_r = 6$ (shown in Fig. 4). It is observed that when using the PSFs corresponding to the right permittivity value the OUTs are reconstructed well at the true positions at each plane.

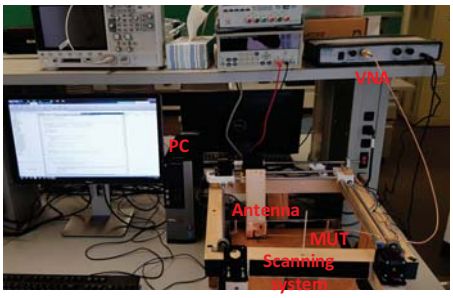

(a)

(b) (c)

Fig. 5. (a) Experimental setup, (b) MUTs, and (c) UWB antenna.

B. *Experimental Results*

Fig. 5(a) shows the experimental setup including: material under test (MUT), two stepper motors for positioning along the x and y axes, Arduino Uno board with Adafruit motor shield v2.3 for the motor control via PC, an ultrawide band (UWB) antenna manufactured by SMAKN [7] operating from 2.8 GHz to 11 GHz, and an Anritsu Shockline vector network analyzer (VNA) model MS46322B. Three types of MUTs are employed as shown in Fig. 5(b) with size of 30 cm × 30 cm, which include hardwood, foam which makes up ceiling tiles, and medium-density fiberboard (MDF). They are expected to have relative permittivities in the range of 1 to 3. Fig. 5(c) shows the UWB antenna placed inside a metal cavity with size of 6 cm × 5.5 cm × 4 cm for directing the microwave power toward the MUTs and reducing backward interferences. In the data acquisition process, MUT is stationary while antenna is scanning over a rectangular aperture with the size of 23 cm × 17 cm. The sampling steps are 40 along x direction and 30 along y direction.

We implement holographic imaging technique over two depths of 14 mm and 42 mm deep inside these MUTs. Thin copper plates with size of 4 cm × 2.5 cm are used as objects to be imaged. For each MUT, two of the objects are placed around the origin along x at the depth of 14 mm with an approximate center-to-center distance of 8 cm between them. Another object is placed approximately at the center at the depth of 42 mm.

Based on the proposed technique, all the measurements are implemented at two sets of frequencies. The first set has 20 frequencies uniformly distributed over the range of 3 GHz to 8 GHz. The second set has 20 frequencies uniformly distributed over the range of 3.5 GHz to 7.5 GHz. We first perform image reconstruction on responses at these two sets of frequencies to obtain two sets of images and evaluate the total error E_T as described in section II.

Here, for all image reconstructions, in order to reduce high frequency noise, we adjusted the maximum values of Fourier variables k_x and k_y. Besides, the image guided filtering [8] in MATLAB is applied using *imguidedfilter* function to further

TABLE I
TOTAL ERROR (E_T) WHEN RECONSTRUCTING IMAGES WITH VARIOUS PSFS FOR THE THREE MEASURED MATERIALS

Material	PSF for MDF	PSF for Foam	PSF for Wood
MDF	4.58	10.97	11.77
Foam	2.51	1.50	2.92
Wood	1.25	3.27	1.00

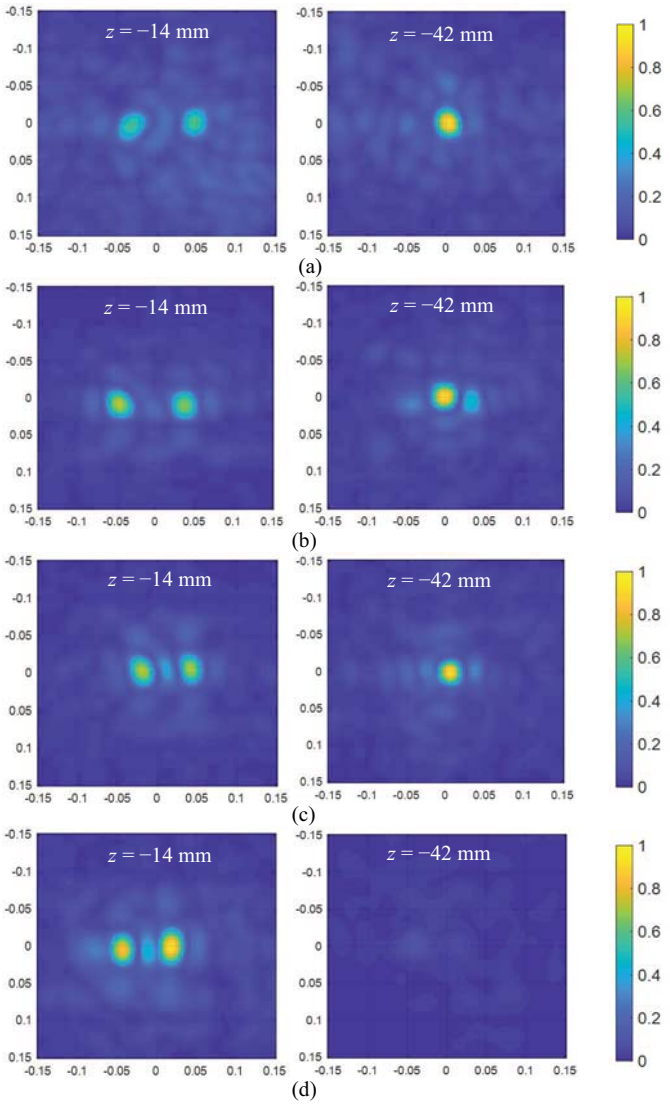

Fig. 6. Reconstructed images for: (a) MDF using PSFs corresponding to MDF, (b) wood using PSFs corresponding to wood, (c) foam using PSFs corresponding to foam, and (d) foam using PSFs corresponding to MDF. Horizontal axis: x (mm), vertical axis: y (mm).

reduce the background artifacts in the images. This method performs edge-preserving smoothing.

Table I shows the computed E_T values. It is observed that when using the PSFs corresponding to the same MUT, the error is minimum validating the proposed algorithm.

Figs. 6(a)-(c) shows the reconstructed images when using the corresponding PSFs for each MUT. It is observed that the objects are reconstructed well at their true positions. Due to the slight differences in the placement of the thin copper plates for each experiment, the reconstructed images of the objects show slight differences. Then, Fig. 6(d) shows the reconstructed images of objects inside the foam using PSFs corresponding to MDF. It is observed that two thin copper plates can be reconstructed at the depth of $z = -14$ mm with slightly stronger background artifacts and the degraded cross-range resolution (the bright spots due to the objects appear slightly wider). Besides, the single object on the plane $z = -42$ mm cannot be reconstructed at all. Overall, it is observed that when the assumed background medium property is not right, OUTs are not reconstructed well and the image quality degrades. In general, when the employed PSFs do not correspond to the true MUT, the matrix of coefficients for the system of equations in (3) is not accurate. This leads to errors in the solutions and can potentially lead to the image quality degradation in both range and cross-range directions.

IV. CONCLUSION

In this paper, a technique for estimation of background medium's dielectric properties is proposed using microwave holographic imaging. This technique first determines a possible range of values for the properties ε and σ. Then at each assumed property pair (ε, σ) within that range, compares two sets of images obtained from the recorded data at two frequency sets and obtains a total error at each assumed property pair (ε, σ). The error is minimum at the estimated values of the dielectric properties ε and σ. Simulation and experimental results validated the proposed technique. It can be employed in various applications for 3D imaging of objects hidden in homogeneous media.

ACKNOWLEDGMENT

This project has been supported by US national science foundation (NSF), award No. 1920098, and New York Institute of Technology's (NYIT) Institutional Support for Research and Creativity (ISRC) Grants.

REFERENCES

[1] N. K. Nikolova, "Microwave near-field imaging of human tissue and its applications to breast cancer detection," *IEEE Microwave Mag.*, vol. 12, no. 7, pp. 78–94, Dec. 2011.

[2] R. Appleby and H. B. Wallace, "Standoff detection of weapons and contraband in the 100 GHz to 1 THz region," *IEEE Trans. on Antennas and Propag.*, vol. 55, pp. 2944–2956, 2007.

[3] K. M. Yemelyanov, N. Engheta, A. Hoorfar, and J. A. McVay, "Adaptive polarization contrast techniques for through-wall microwave imaging applications," *IEEE Trans. on Geoscience and Remote Sensing*, vol. 47, no. 5, pp. 1362–1374, May 2009.

[4] R. Zoughi, *Microwave Non-Destructive Testing and Evaluation*. Kluwer Academic Publishers, 2000.

[5] D. M. Sheen, D. L. McMakin, and T. E. Hall, Near-field three-dimensional radar imaging techniques and applications," *Applied Optics*, vol. 49, no. 19, pp. E83–E93, Jun. 2010.

[6] R. K. Amineh, N. K. Nikolova, M. Ravan, *Real-Time Three-Dimensional Imaging of Dielectric Bodies Using Microwave/Millimeter Wave Holography*. Wiley-IEEE Press, 2019.

[7] Ultra Wide band UWB+1S Antenna 2.8 GHz - 11 GHz for UWB TX/RX SDR RADAR GPR SIGINT EMC TEST ADSB WIFI FVP DRONE VIDEO VIVALDI ANTENNA Manufacturer: SMAKN, Amazon.com: SMAKN: Electronics

[8] K. He, J. Sun, and X. Tang, "Guided image filtering," *IEEE Trans. Pattern Analysis and Machine Intelligence*, vol. 35, no. 6, pp. 1397−1409, Jun. 2013.